RESEARCH ON THE MECHANISM OF ENERGY ATTENUATION AND COMPENSATION DURING THE SERVICE-LIFE OF OXYGEN LANCE NOZZLES

Junnan LI[1], Kun LIU[1*], Guangqiang LIU[2], Peng HAN[1], Yuanxin LIU[2,3]

[1] School of Materials and Metallurgy, University of Science and Technology Liaoning, Anshan, Liaoning 114051, China

[2] School of Civil Engineering, University of Science and Technology Liaoning, Anshan, Liaoning 114051, China

[3] Technology Centre, Benxi Steel Group Corporation, Benxi, Liaoning 117100, China

[*] Corresponding author; E-mail: liukun0206@sina.com

In the high-temperature environment inside the converter, the holes of oxygen lance nozzles will gradually be damaged with the increase in the number of blowing times. Therefore, clarifying the characteristics of nozzle jet and the variation of energy attenuation with the increase in number of blowing times is of great guiding significance for top-blown converter steelmaking. In the present work, the 120t converter 5-hole oxygen lance nozzle was taken as the research object, and the jet of nozzles with different damage morphologies were calculated. The jet characteristics and energy attenuation under different blowing heats were comprehensively explored. The results indicated that the wear at the exit of nozzle caused strong fluctuations in the jet, and the energy dissipation during the oscillation stage increased with the increase in the degree of wear. When the blowing heat lied within the range of 241-300, the energy consumption of jet oscillation reached up to 20.31%. A mathematical model was established for the correlation of number of blowing times, oxygen lance heights, and effective impact area. Based on the evaluation index of effective impact area, a compensation scheme for oxygen lance heights and pressure was proposed. The research results provide reference for the rational and efficient use of oxygen lance in industrial smelting.

Key words*: oxygen lance; operational life; jet energy attenuation; compensation mechanism*

1. Introduction

During converter smelting, the Laval tube of the oxygen lance nozzle jets oxygen into the molten pool at supersonic speed to achieve the purposes of stirring, oxygen supply, decarbonization and dephosphorization [1-3]. Therefore, the jet characteristics of the oxygen lance have a significant impact on the effectiveness of converter steelmaking. Currently, research on the jet behavior and the interaction with the molten pool of oxygen lance nozzles has been very thorough. In terms of jet hydrodynamics, researchers have explored the effects of various parameters such as inlet pressure and ambient temperature on jet attenuation and aggregation [4-7]. The results showed that an increase in

the inlet pressure and ambient temperature led to an increase in the length of jet core zone and a slower attenuation of the jet, with the operational pressure having a relatively minor impact on the aggregation of multiple jets. In terms of the interaction between the jet and the molten pool, previous studies have shown that, with the increase in lance height, the impact depth of the jet on the molten pool became shallower, the impact area increased, and the flow in the molten pool weakened [8-10]. The smelting characteristics of some new types of oxygen lance nozzles have also been studied. Li et al. [11-14] conducted an in-depth study of the jet characteristics of a swirling flow oxygen lance, and the corresponding results showed that, under the same conditions, the swirling flow oxygen lance had a larger impact area than the traditional oxygen lance, with a shallower and wider cavity. Meanwhile, the swirling flow oxygen lance generates significantly less splashing at the converter mouth compared to traditional oxygen lance. Liu et al. [15-18] studied the smelting characteristics of a dual-parameter oxygen lance, and the corresponding results revealed that the optimized dual-parameter oxygen lance formed deeper and wider cavities than those observed in traditional nozzle. In industrial applications, the dual-parameter oxygen lance has increased intensity of oxygen supply and rate of dephosphorization, shortened blowing time, and reduced oxygen consumption.

However, it is well-known that, during the smelting process, the nozzle is subject to multiple factors such as high temperature radiation, furnace gas scour, slag splashing, and the temperature difference between the internal cooling water and the external environment, all of which result in varying degrees of wears to the nozzle hole outlet, causing the working conditions of the oxygen lance to deviate from the designed parameters, changing the jet characteristics, and affecting the smelting process. In recent years, the jet behavior of worn nozzles has gradually been taken seriously. Garajau et al. [19] argued that, when the operating pressure was lower than the designed pressure, the wear at the nozzle was caused by backflow and combustion at the outlet of nozzle holes, resulting in melting of copper around the outlet of nozzle holes. Feng and Lv et al. [20, 21] investigated the jet characteristics of worn nozzles and its stirring effect on the melt pool. Their results showed that, with the increase in the degree of nozzle wear, the jet velocity attenuated faster, the impact area gradually decreased, the impact depth on the molten pool decreased, and the dead zone area of the molten pool increased.

In summary, current research on the blowing characteristics of worn nozzles have mainly focused on varying depths or widths of wear at the outlet of nozzle. However, the relationship between the depth or width of wear and the number of blowing heat is not clear. Based on on-site measurements, it has been found that the depth and width of wear do not vary linearly with the number of blowing heats. Establishing a quantitative relationship between the blowing characteristics of worn nozzles and the number of blowing heats, and clarifying the variation pattern of the dissipation of jet's energy throughout the service-life of the nozzle is of great significance for guiding the compensation of lance heights and pressure of worn nozzles in actual blowing processes.

In the present study, a 5-hole oxygen lance used in a 120t converter is taken as the research object. The quantitative relationship between the wear morphology of the nozzle and the blowing heat is established throughout the entire life-cycle of the nozzle. The jet energy of the nozzle throughout the entire life-cycle is analyzed through numerical simulation. The correlation among the number of blowing times, effective impact area, and lance height is established. Compensation mechanisms under different blowing heats are also proposed. The research results provide reference for the efficient use of oxygen lance in industrial production.

2. Numerical model

2.1. Assumptions

(1) Oxygen was assumed to be an ideal compressible Newtonian fluid with a constant specific heat.

(2) The flow was stable, and consisted of a compressible, non-isothermal process.

(3) The nozzle was a smooth-walled surface, whereas friction was ignored.

2.2. Governing equations

Mass conservation equation [22-24] is given by Eq. (1).

$$\frac{\partial\left(\rho u_i\right)}{\partial x_i}=0 \tag{1}$$

where ρ is the fluid density [kgm^{-3}], conforming to the ideal gas equation of state of: $p=\rho RT$, and u_i is the i directional velocity [ms^{-1}].

Momentum conservation equation is given by Eq. (2) and (3).

$$\frac{\partial\left(\rho u_i u_j\right)}{\partial x_j}=-\frac{\partial p}{\partial x_i}+\frac{\partial\left(\tau_{ij}-\rho\overline{u_i u_j}\right)}{\partial x_j} \tag{2}$$

$$\tau_{ij}=\mu\left(\frac{\partial u_j}{\partial x_i}+\frac{\partial u_i}{\partial x_j}-\frac{2\partial u_k}{3\partial x_k}\delta_{ij}\right) \tag{3}$$

where u_j is the j directional velocity [ms^{-1}], p denotes the pressure [Pa], τ_{ij} is the intermolecular viscous stress [Pa], δ_{ij} represents the Kronecker delta, μ is the molecular viscosity [Pa·s], and the Reynolds stress term $-\rho\overline{u_i u_j}$ represents the influence of turbulence and is described according to the Boussinesq approximation, as given by Eq. (4).

$$-\rho\overline{u_i u_j}=\mu_t\left(\frac{\partial u_j}{\partial x_i}+\frac{\partial u_i}{\partial x_j}\right)-\frac{2}{3}\left(\rho k+\mu_t\frac{\partial u_k}{\partial x_k}\right)\delta_{ij} \tag{4}$$

where μ is the turbulent viscosity, and k denotes the turbulent kinetic energy [m^2/s^2].

Energy conservation equation is given by Eq. (5).

$$\frac{\partial\left[u_i\left(\rho C_p T+p\right)\right]}{\partial x_i}=-\frac{\partial}{\partial x_i}\left(\lambda\frac{\partial T}{\partial x_i}+\frac{C_p\mu_t}{\mathrm{Pr}_t}\frac{\partial T}{\partial x_i}\right)+\frac{\partial}{\partial x_i}\left(\tau_{ij}u_j-u_j\rho\overline{u_i u_j}\right) \tag{5}$$

where λ is the thermal conductivity [Wm^{-1}K^{-1}], C_p represents the specific heat capacity at constant pressure [Jkg^{-1}K^{-1}], whereas Pr_t is defined as the ratio of momentum vortex diffusivity to heat transfer vortex diffusivity, with value of 0.85.

2.3. Turbulence model

Li et al. [25, 26] investigated the influence of turbulence models on jet characteristics at different temperatures, and the results showed that the standard $k-\omega$ model could more accurately calculate the behavior of multiple jets at high temperatures. Therefore, the standard $k-\omega$ model was used in the present paper, which is given by Eq. (6) and (7).

$$\frac{\partial\left(\rho k u_j\right)}{\partial x_j}=\frac{\partial}{\partial x_j}\left[\left(\mu+\frac{\mu_t}{\sigma_k}\right)\cdot\frac{\partial k}{\partial x_j}\right]+G_k-Y_k+S_k \tag{6}$$

$$\frac{\partial\left(\rho\omega u_j\right)}{\partial x_j}=\frac{\partial}{\partial x_j}\left[\left(\mu+\frac{\mu_t}{\sigma_\omega}\right)\cdot\frac{\partial\omega}{\partial x_j}\right]+G_\omega-Y_\omega+S_\omega \tag{7}$$

where σ_k=2.0, σ_ω=2.0, and μ_t is the turbulent viscosity [Pa×s], as given by Eq (8).

$$\mu_t=\frac{\rho k}{\omega} \tag{8}$$

where S_k and S_ω represent the user-defined source terms, G_k denotes the turbulent kinetic energy due to average velocity gradient, and G_ω represents the generation of specific dissipation rate, as given by Eq. (9) and (10).

$$G_k=-\rho\overline{u_iu_j}\frac{\partial u_j}{\partial x_i} \tag{9}$$

$$G_\omega=-\rho\overline{u_iu_j}\frac{\omega}{k}\frac{\partial u_j}{\partial x_i} \tag{10}$$

where Y_k and Y_ω represent the dissipations of k and ω due to turbulence, which are calculated using Eq. (11) - (14).

$$Y_k=\beta_1\rho k\omega \tag{11}$$

$$Y_\omega=\beta_2\rho\omega^2 \tag{12}$$

$$\beta_1=0.09\left(1+1.5F\left(M_t\right)\right) \tag{13}$$

$$\beta_2=0.072\left(1-1.875F\left(M_t\right)\right) \tag{14}$$

where $F(M_t)$ is a compressible function, expressed by Eq. (15).

$$F\left(M_t\right)=\begin{cases}0 & \frac{2k}{a^2}\le 0.25\\ \frac{2k}{a^2}-0.0625 & \frac{2k}{a^2}>0.25\end{cases} \tag{15}$$

where a is the speed of sound, as given by Eq. (16).

$$a=\sqrt{\gamma RT} \tag{16}$$

2.4. Computational domain and boundary conditions

The modeling parameters of 5-hole oxygen lance for 120t converter are presented in Tab. 1, whereas Fig. 1 shows the schematic of the oxygen lance. According to previous reports, the service-life of the nozzle in a steelmaking plant is about 300 heats. The wear morphology of nozzle holes under different blowing heats is shown in Fig. 2. For the convenience of analysis, the present study assumed that the exit of worn nozzle was a regular circle, whereas the measuring point was the most severely damaged position. The depth of the wear and the diameter of the nozzle after wear were measured using vernier calipers. The wear depth was defined as the vertical distance from the worn point to the outlet of the nozzle. For the convenience of geometric modeling, the wear width was

defined as the half of the difference between the diameter of the worn nozzle's outlet and the diameter of the nozzle's outlet. Therefore, the wear depth and wear width of each nozzle hole of 10 nozzles (50 holes in total) were randomly measured in 60 blowing heats, and the average values were taken to establish the geometric parameters of the worn nozzle holes, as presented in Tab. 2. The corresponding measured values are shown in Fig. 3, whereas the geometric model is shown in Fig. 4.

Table1. Structural parameters of 5-hole oxygen lance

Nozzle structure	Throat diameter, d*/mm	Outlet diameter, de/mm	Inclination angle, a/°	Expansion Angle, β/°
Parameters	39.5	51.8	14.5	8.2

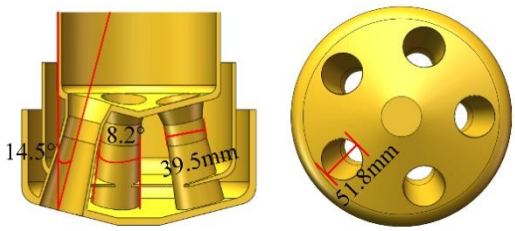

Figure 1. Schematic of the oxygen lance

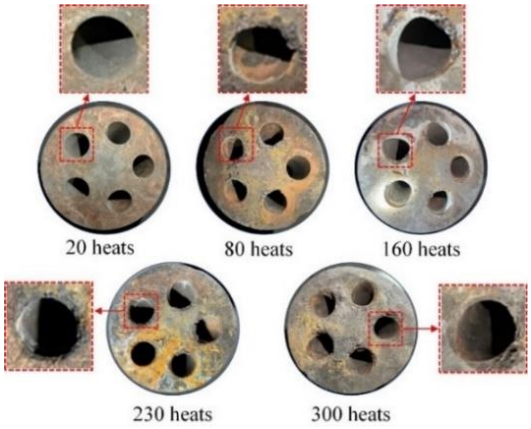

Figure 2. Damage morphology of nozzle holes under different heats

Table 2. Geometric modeling parameters for the degree of wear under different heats

Scheme label	Blowing times	Wear depth (mm)	Wear width (mm)
(a)	0	0	0
(b)	1-60	4.08	0.99
(c)	61-120	7.74	2.37
(d)	121-180	12.63	3.82
(e)	181-240	13.12	4.66
(f)	241-300	15.61	7.57

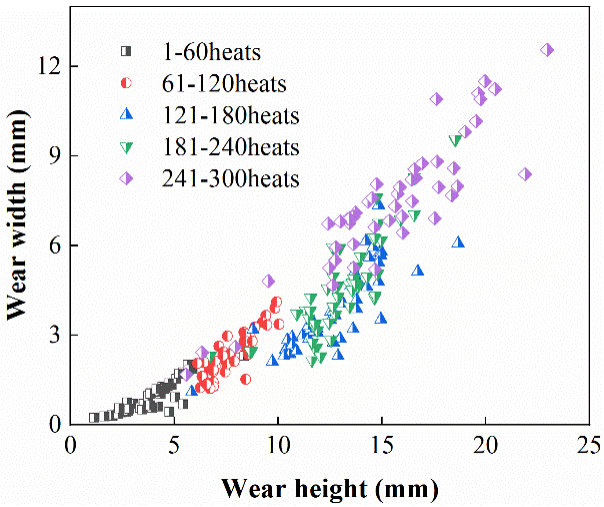

Figure 3. Measurements of holes' wear depths and wear widths under different heats

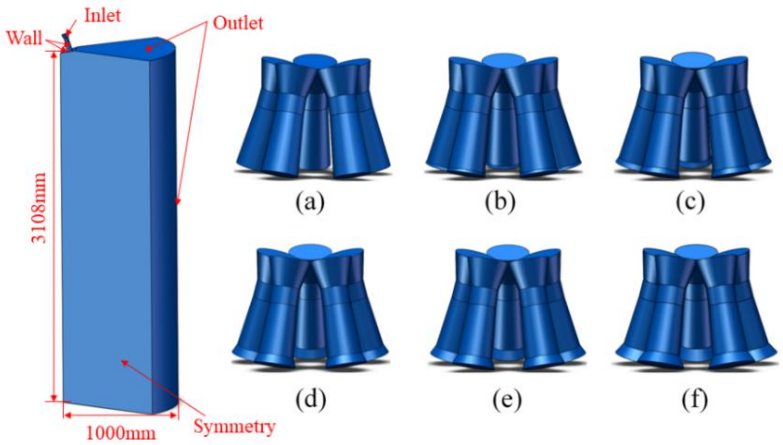

Figure 4. Geometric model and calculation domain of nozzle holes under full service-life

In order to reduce the computational complexity, 1/5 of the nozzle was calculated and periodic boundary conditions were set. Structured grid was performed on the computational domain, and the damaged areas of the nozzle holes were dense. When the number of grids was 4 million and 4.7 million, the number of grids had little influence on the calculated results. Therefore, the number of grids in the calculations was set to be 4 million. ANSYS Fluent 2021R1 was used to converge the solution. Using standard wall functions to treat near the surfaces of walls, all normal gradients were set

Table 3. Boundary condition parameters

Inlet pressure	Inlet flow rate (one nozzle)	Inlet temperature	Ambient temperature	Back pressure
0.82 MPa	7200 Nm^3h^{-1}	300 K	1873 K	0.104 MPa

to be zero. The continuity, momentum and energy equations for the flow terms, turbulent kinetic energy and turbulent dissipation rate were used in a second-order windward format using a coupled pressure-velocity solver with energy residuals of less than 10^{-6} and residuals of less than 10^{-3} for the other variables considered to be converged. Moreover, SIMPLE algorithm was used to solve the

coupling between pressure and velocity. Tab. 3 presents the boundary conditions set for the simulation in the current work.

2.5. Validation of the model

The selection of turbulence models was based upon some current works. Wang et al. [10] verified that the standard k-ω model was more accurate in calculating the behavior of multiple jet streams. Similarly, Li et al. [1, 27] reported similar results in their works. Li et al. [26] compared the simulation results with experimental results and found that the standard k-ω model outperformed other models in simulating high-temperature supersonic jets. Zhao et al. [28] used the SST k-ω model to simulate the jet's behavior at different preheating temperatures, and conducted relevant experiments to verify the accuracy of the model. Meanwhile, Feng et al. [18, 29] used the standard k-ε model to simulate the oxygen lance jet behavior.

In order to ensure the accuracy and effectiveness of the numerical simulation, it is necessary to verify the model. The present article conducted experimental verification on the selected turbulence model. The experimental data was based on experiments conducted by Sumi et al. [25] in a high-temperature furnace with a single-hole water-cooled nozzle. The temperature inside the furnace was recorded by 8 thermocouples. The dynamic pressure, temperature, and gas density of the jet were measured and calculated using a pitot tube. The velocity was obtained through calculations. In the present paper, Sumi's experimental nozzle was used as the model. The software package of SolidWorks was used to establish the three-dimensional geometric model of the single-hole nozzle. Numerical simulations were carried out based on standard k-ω, standard k-ε, SST k-ω, realizable k-ε models. For verification purposes, the central line velocity of the jet was compared with the experimental data reported in a previous work [25]. The corresponding results are shown in Fig. 5. The calculated results of the standard k-ω turbulence model were close to the experimental values, and the variation trend was consistent. Compared to standard k-ε model, the standard k-ω turbulence model had reduced the errors at four measurement points by 36.24%, 20.8%, 19.01%, and 15.33%, which verified the accuracy of the standard k-ω model selected in the present research.

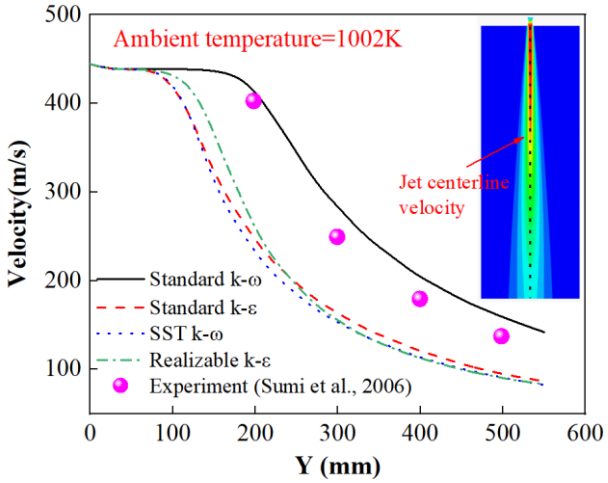

Figure 5. Validation of the proposed model [25]

3. Results and discussion

3.1. Jet characterization and energy analysis

Fig. 6 shows the contours of jet velocity of the nozzle during its service-life. The results showed that the worn nozzle generated shock waves at the outlet of the nozzle. This was because the oxygen in the expansion section of the Laval tube underwent a process of pressure reduction and acceleration. The pressure at the damaged nozzle was greater than the ambient pressure, resulting in an under-expansion state of the jet at the outlet and an expansion wave at the worn area. As the number of blowing heats increased, more violent fluctuations were produced by the jet. Based upon the values calibrated at 40de, it was found that, with the increase in the degree of wear, the range of the jet decreased gradually. When the nozzle blowing range was 1-60 times, the jet width was reduced by 20%. When the number of blowing lied within the range of 61-120 t imes, the jet width decreased by 26.67%. When the number of blowing lied within the range of 121-240 times, the jet width was reduced by 28.89%. When the nozzle was blown for 241-300 times, the jet width was reduced by 35.56%. The width of jet decreased with the increase in the number of blowing heats, indicating that the impact area decreased with the increase in the number of blowing heats. In addition, from the jet at 60de, it can be found that the jet cohesion gradually weakens with the increase in the number of blowing heats.

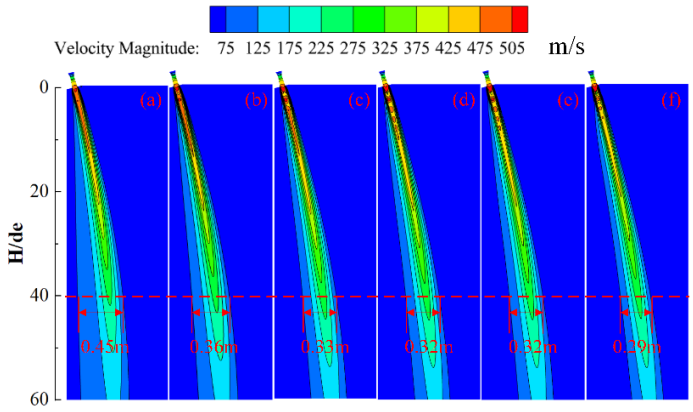

Figure 6 Nozzle jet velocity contours during its service-life

Fig. 7 shows the maximum velocity line diagram for each cross-section of the jet. As shown by Zone A in Fig. 7, as the degree of nozzle wear increased, the velocity fluctuation at the outlet became more intense. Compared with Scheme a, the maximum speeds of Schemes b, c, d, e, and f increased by 2.63%, 7.58%, 14.03%, 14.92% and 16.97%, respectively. The jet tended to stabilize when entering Zone B. When the number of blowing was more than 120, the attenuation of jet velocity caused by shock waves accelerated. Compared with the jet velocity of the unworn nozzle, the jet velocities for the numbers of blowing of 121-180, 181-240, and 241-300 decreased by 4.11%, 4.83%, and 6.67%, respectively. When the jet entered the range of H=35de-45de, the centerline velocity of the unworn oxygen lance jet was the smallest, while the attenuation was the fastest. The jet width marked in Fig. 6 also intuitively showed that the worn nozzle was not easy to expand radially, resulting in slower attenuation of the centerline velocity of the jet.

In order to clarify the energy dissipation of the oscillating section caused by the shock waves of the oxygen lance jet with the worn nozzle, the length of the oscillating section of the jet during the service-life of nozzle was investigated and the corresponding energy analysis was carried out. In the

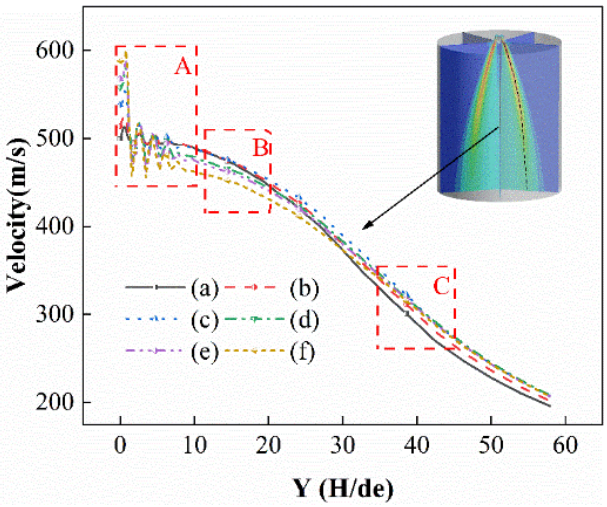

Figure 7. Maximum velocity of each cross-section of the jet

present paper, two conditions were required for the length of the oscillating section. The velocity of the center line of the jet decreased gradually from the end of the oscillating section. The centerline velocity of the jet, which was measured at distances of 5 cm in the axial direction and after stabilization, had a difference of less than 3 m/s between adjacent cross-sections. The lengths of the oscillating section and the supersonic section are shown in Fig. 8 (1). As shown in Fig. 8 (1), the length of the oscillating section increased with the increase in the number of blowing times, whereas the length of the supersonic section first increased, and then, decreased with the increase in the number of blowing times. Fig. 8 (2) shows the kinetic energy and the rate of loss of kinetic energy in the oscillating section. The kinetic energy is the kinetic energy integral of the section at the end of the oscillating section. The rate of loss of kinetic energy in the oscillating section is calculated by Eq. (17),

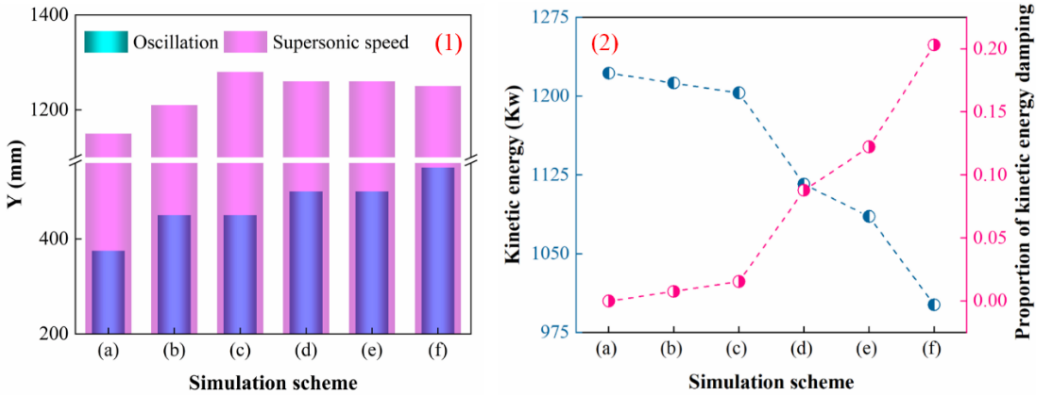

Figure 8. (1) Left: Length of jet's oscillating and supersonic sections; (2) Right: Kinetic energy of jet and rate of loss of kinetic energy

where Ek_s is the rate of loss of kinetic energy, and Ek_0 and Ek_n are the integrals of the kinetic energy at the end of the oscillating section at 0 and numbers of blowing heat, respectively. The results indicated that, as the degree of wear increased, the kinetic energy of the end surface of the oscillating section gradually decreased, whereas the rate of loss of kinetic energy caused by jet under-expansion gradually increased. The energy loss rates in the oscillating section were 0.77%, 1.55%, 8.77%, 12.22%, and 20.31% for the numbers of blowing heats of 0-60, 61-120, 121-180, and 241-300, respectively.

$$Ek_s = \frac{Ek_0 - Ek_n}{Ek_0} \times 100\% \quad (17)$$

The analysis of the impact area can clarify the characteristics of the jet when it reaches the molten pool. In the present study, a dynamic pressure of greater than 4000 Pa [3] was defined as the effective impact area (i.e., the area where the jet blew away the slag layer and chemically reacted with the molten steel). The relationship between the effective impact area and the number of blowing times at different lance heights is shown in Fig. 9. The results showed that the lance position with the maximum effective impact area under different blowing heats was 40de. When the lance position was less than 40de, the effective impact area gradually decreased with the increase in the number of blowing times. When the lance position was higher than 40de, the effective impact area exhibited a quadratic relationship with the number of blowing heats. This was due to the radial entrainment effect in the unworn nozzle, which was stronger than the jet velocity attenuation caused by the damaged nozzle, resulting in the lance heights of more than 40de. Meanwhile, the effective impact area increased within the number of blowing times of 120, after which, it gradually decreased.

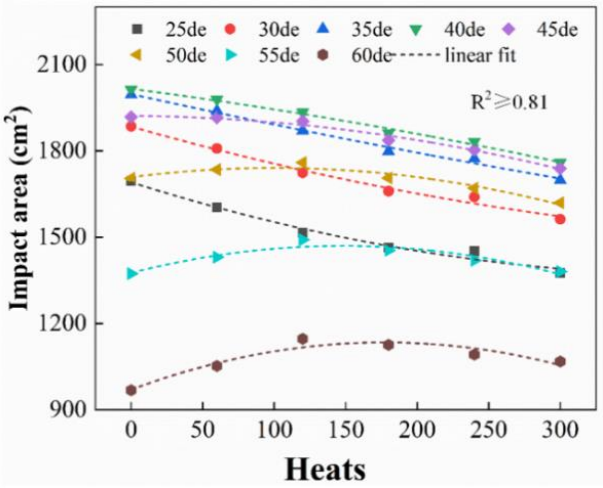

Figure 9. Relationship between effective impact area and number of blowing heat and lance height

In order to explore the relationship among lance height, number of blowing heat and effective impact area, the effective impact area and the number of blowing heat at various lance heights were fitted, and the corresponding results are given by Eq. (18). The fitting coefficients at different lance heights are presented in Tab. 4. The n^2 coefficient in the defined equation was represented by *B2*, whereas the coefficient *n* was represented by *B1*. Additionally, *B3* represented the constant term. Furthermore, *B1*, *B2*, and *B3* were fitted twice, and the corresponding fitting results are shown in Fig. 10, which are also substituted in Eq. (18). Finally, a mathematical model for the effective impact area between the number of blowing heat and the nozzle height was established, as given by Eq. (19).

$$s_n = B2 * n^2 + B1 * n + B3 \quad (18)$$

Table 4. Fitting coefficients at different lance heights

Lance heights	B1	B2	B3
25de	-1.5723	0.0019	1690.5025
30de	-1.4168	0.0013	1884.2095
35de	-1.0977	0.0004	1996.9525
40de	-0.6467	-0.0007	2015.3173
45de	-0.0280	-0.0020	1920.9932
50de	0.6399	-0.0032	1780.3105
55de	1.2660	-0.0043	1375.8014
60de	1.8547	-0.0052	969.7052

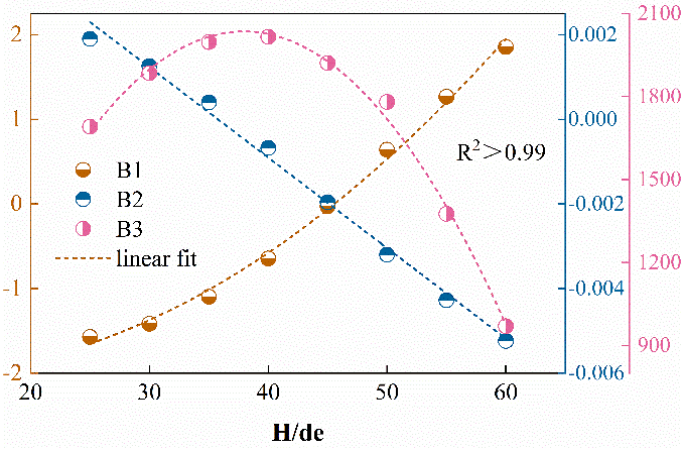

Figure 10. Quadratic fitting of effective impact area to blowing heats at different lance heights

$$\begin{cases} \dfrac{s_n}{S_0} = \dfrac{B2*n^2 + B1*n + B3}{C} *100\% \\ B1 = 0.0016\left(H/de\right)^2 - 0.03(H/de) + 1.88 \\ B2 = -2.14E^{-4}(H/de) + 0.0076 \\ B3 = -2.17(H/de)^2 + 164.97(H/de) - 1094.55 \\ C = cons\tan t \end{cases} \tag{19}$$

3.2. Jet compensation mechanism during the service-life of oxygen lance

As mentioned above, worn nozzle holes affected the jet characteristics. Due to this reason, the present study took the effective impact area as an index, and used both the lance height and pressure compensation to reduce the jet deviation due to the damage of nozzle holes. Fig. 11 shows the critical blowing times for nozzle height compensation within the range of 30de - 45de. The present paper defined the effective compensation of lance height and pressure after wear as a deviation of the effective impact area within $\pm$ 5%, as shown by the gray area in Fig. 11. At 30de, the critical number of blowing times that can be compensated by the lance height was about 274. At 35de, the critical number of blowing times was about 159. At 40de, the critical number of blowing times was about 141, whereas at 45de, the critical number of blowing times was about 240.

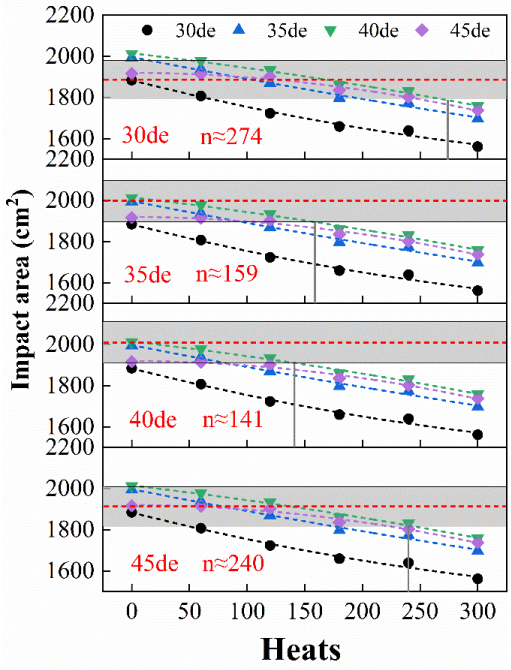

Figure 11. Relationship among effective impact area, lance height's compensation and critical blowing times

When the number of blowing heat was greater than the critical number of blowing heat, the blowing deviation caused by nozzle holes' wear could not be compensated by lance height. Due to this reason, the pressure compensation mechanism was explored. Fig. 12 shows the velocity contour for 30de cross-section under different pressures in different blowing heats. When the pressure was held at a certain value, the impact area decreased gradually with the increase in the number of blowing heat. At the same degree of wear for the nozzle holes, the impact area increased with the increase in pressure. Taking the contours labelled within the red boxes in Fig. 12 as examples, the morphology of

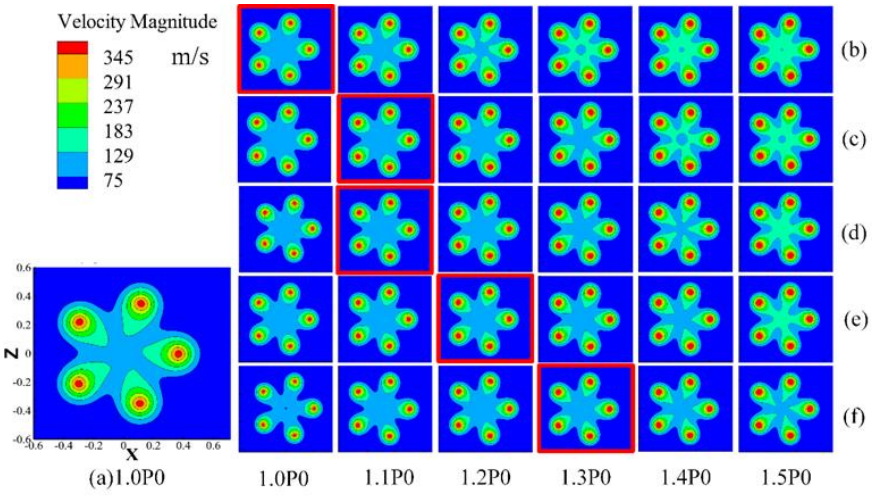

Figure 12. Cross-sectional velocity contours at 30de for different inlet pressures

the impact area within the $1.0P_0$ (P_0 represents the design pressure of the nozzle) and 60 number of blowing heat was similar to those for $1.1P_0$ and 61-180 number of blowing heat, $1.2P_0$ and 181-240 number of blowing heat, and $1.3P_0$ and 241-300 number of blowing heat. Through quantitative

analysis of the area enclosed by the velocity of V=183 m/s, it was found that the areas of unworn nozzle hole at $1.0P_0$ (Scheme a), 1-60 number of blowing heat at $1.0P_0$ (Scheme b), 61-180 number of blowing heat at $1.1P_0$ (Schemes c and d), 181-240 number of blowing heat at $1.2P_0$ (Scheme e), and 241-300 number of blowing heat at $1.3P_0$ (Scheme f) were 0.15 m^2, 0.14 m^2, 0.15 m^2, 0.14 m^2, 0.15 m^2, and 0.15 m^2, respectively. This demonstrates the feasibility of compensating for the impact area of the worn nozzle by increasing the inlet pressure.

Figure 13 shows the pressure compensation scheme under different numbers of blowing heat. The calculated deviation of the effective impact area of Scheme b from the unworn oxygen lance was less than 5%. Therefore, Fig. 13 shows the pressure compensation mechanism for Schemes c-f. The results showed that, when the lance height was 30de, the maximum compensation pressure reached $1.3P_0$, whereas for the lance height of 35de, the maximum compensation pressure was $1.2P_0$. When the lance height was 40-45de, the maximum compensation pressure was $1.1P_0$. As can be seen from Fig. 11, with the increase in lance height, the slope between the effective impact area and the number of blowing times gradually decreased. Therefore, the wear of nozzle holes at low lance heights had a greater impact on the effective impact area, which also explained the phenomenon that the compensation pressure increased with the decrease of lance height.

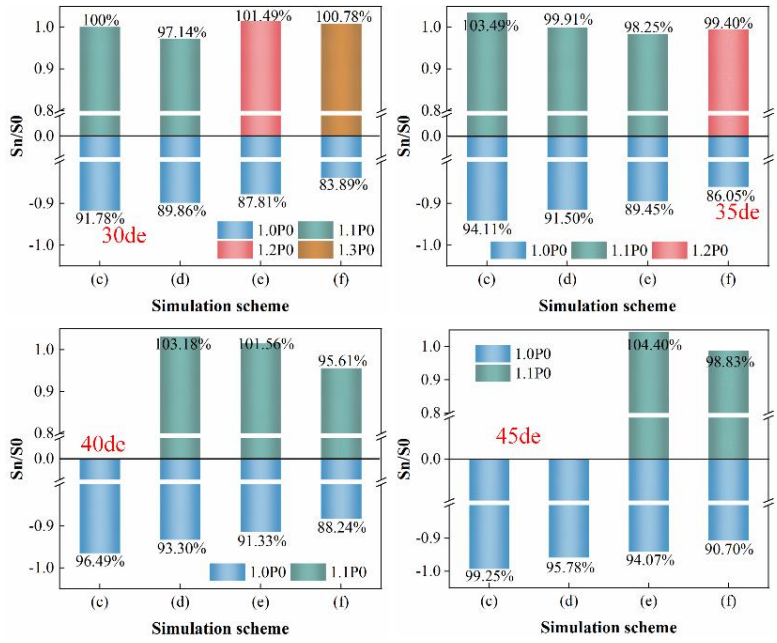

Figure 13. Pressure compensation scheme under different numbers of blowing heat

4. Conclusions

(1) The worn nozzle was under-expansion jet, resulting in more violent jet fluctuations with the increase in the number of blowing heat, and the jet width was reduced.

(2) With the increase in the number of blowing heat, the energy loss in the oscillating section of the jet gradually increased. Within the number of blowing heat of 300, taking the number of blowing heat of 60 as a unit, the rates of losses of energy for the oscillating section were 0.77%, 1.55%, 8.77%, 12.22% and 20.31%, respectively.

(3) The mathematical correlation among the number of blowing heat, blowing lance height and the effective impact area was established. The correlation between the lance height and the pressure

compensation scheme under different numbers of blowing heat was also proposed. Under the optimum lance height of 40de, about 141 was the critical number of blowing heat for lance height's compensation, whereas the pressure compensation method of increased the inlet pressure to $1.1P_0$ that can be adopted for numbers of blowing heat of more than about 141.

Acknowledgments

The Education Department Project of Liaoning Province (JYTMS20230932). The National Natural Science Foundation of China (U20A20272). Fundamental Research Funds for the Liaoning Universities (LJ212410146002).

References

[1] Li, M. M., *et al.*, Effect of operation parameters on supersonic jet behaviour of BOF six-nozzle oxygen lance, *Ironmaking & Steelmaking*, *41* (2014), 9, pp. 699-709

[2] Liu, C., *et al.*, Numerical study of the kinetics of dephosphorization with single-flow post-combustion oxygen lance in converter steelmaking process, *Metallurgical and Materials Transactions B*, *55* (2024), 2, pp. 999-1013

[3] Li, J. G., *et al.*, Simulation of flow field of oxygen lance gas jet utilized for 50 t converter, *Journal of Iron and Steel Research International*, *18* (2011), 4, pp. 11-18

[4] Liu, F. H, *et al.*, Flow field characteristic of postcombustion oxygen lance formed by various secondary nozzle arrangements, *Metallurgical and Materials Transactions B*, *55* (2024), 2, pp. 935-949

[5] Dong, P. Y., *et al.*, Numerical study on gas-metal-slag interaction with single-flow postcombustion oxygen lance in the steelmaking process of a top-blown converter, *JOM*, *74* (2022), 4, pp. 1509-1520

[6] Dong, P. Y., *et al.*, Simulation and application of post-combustion oxygen lance in a top-blown converter, *Ironmaking & Steelmaking*, *50* (2023), 1, pp. 55-66

[7] Dong, P. Y., *et al.*, Research on nozzle design and application of single-flow postcombustion oxygen lance in a 120 t top-blown converter, *Steel Research International*, *92* (2021), 11, 2100203

[8] Tago, Y., Higuchi, Y., Fluid flow analysis of jets from nozzles in top blown process, *ISIJ International*, *43* (2003), 2, pp. 209-215

[9] Zhang, Y. C., *et al.*, Jet characteristics of a high-mach-number oxygen-lance nozzle under high oxygen pressure, *Metallurgical and Materials Transactions B*, *52* (2021), pp. 4070-4081

[10] Wang, W. J., *et al.*, Three-dimensional compressible flow simulation of top-blown multiple jets in converter, *ISIJ International*, *50* (2010), 4, pp. 491-500

[11] Li, L., *et al.*, Physical and mathematical modeling of swirling gas jets impinging onto a liquid bath using a novel nozzles-twisted lance, *Steel Research International*, *91* (2020), 7, 1900684

[12] Lv, M., *et al.*, Simulation and application of swirl‐type oxygen lance in vanadium extraction converter, *Steel Research International*, *84* (2013), 3, pp. 304-312

[13] Wang, X., *et al.*, Effect of cavity shape caused by jet impact of swirl-type oxygen lance on molten bath mixing efficiency, *Ironmaking & Steelmaking*, *51* (2024), 5,pp. 460-469

[14] Wang, H., *et al.*, Numerical simulation of swirl-type lances in vanadium extraction process, *Chinese Journal of Engineering*, *36* (2014), 1, pp. 89-96

[15] Liu, G. Q., *et al.*, Numerical investigation on behaviors of interlaced jets and their interaction with bath in BOF steelmaking, *AIP Advances*, *9* (2019), 7, 075202

[16] Liu, G. Q., *et al.*, Metallurgical performance of innovative double-parameter oxygen lance in BOF steelmaking, *Ironmaking & Steelmaking*, *48* (2021), 4, pp. 437-446

[17] Liu, G. Q., *et al.*, Splash sheet characteristics induced by the impingement of multiple jets in a steelmaking converter, *Ironmaking & Steelmaking*, *48* (2021), 1, pp. 25-32

[18] Feng, C., *et al.*, Supersonic jet characteristics of two parameter oxygen lance nozzle, *Ironmaking & Steelmaking*, *49* (2022), 1, pp. 109-121

[19] Garajau, F. S., *et al.*, Effects of post-combustion temperature on the wear of the supersonic nozzles in BOF lance tip, *Engineering Failure Analysis*, *96* (2019), pp. 175-185

[20] Feng, C., *et al.*, Effect of nozzle exit wear on the fluid flow characteristics of supersonic oxygen lance, *Metallurgical and Materials Transactions B*, *51* (2020), pp. 187-199

[21] Lv, M., *et al.*, Effect of the wear of supersonic oxygen lance on the stirring characteristics and metallurgical effects in the converter steelmaking process, *Ironmaking & Steelmaking*, *50* (2023), 3, pp. 235-243

[22] Halouane, Y., *et al.*, Turbulent heat transfer for impinging jet flowing inside a cylindrical hot cavity, *Thermal Science*, *19* (2015), 1, pp. 141-154

[23] Ahmadi, H., *et al.*, Numerical modeling of a turbulent semi-confined slot jet impinging on a concave surface, *Thermal Science*, *19* (2015), 1, pp. 129-140

[24] Boucheffa, N., *et al.*, The 2-D plasma thermal jet simulations with substrate interaction, *Thermal Science*, *25* (2021), 5, pp. 3467-3478

[25] Sumi, I., *et al.*, Effect of high-temperature field on supersonic oxygen jet behavior, *46* (2006), 9, pp. 1312-1317

[26] Li, Z. L., Cang, D. Q., Numerical simulation of supersonic oxygen jets at high ambient temperature, *Steel Research International*, *88* (2017), 4, 1600209

[27] Li, M. M., *et al.*, Coalescence characteristics of supersonic jets from multi-nozzle oxygen lance in steelmaking BOF, *Steel Research International*, *86* (2015), 12, pp. 1517-1529

[28] Zhao, F., *et al.*, Behaviors of supersonic oxygen multi-jets with various preheating temperatures, *Metallurgical and Materials Transactions B-Process Metallurgy and Materials Processing Science*, *52* (2021), 4, pp. 2626-2641

[29] Feng, C., *et al.*, Influence of preheating temperature on the characteristics of O^2 + CO^2 jet by mixed injection with a swirling oxygen nozzle, *JOM*, *73* (2021), 10, pp. 2985-2994

Received: 03.10.2024.
Revised: 14.01.2025.
Accepted: 25.06.2025.